Molecular analyses of chorionic-type intermediate trophoblastic lesions: Atypical placental site nodules are closer to placental site nodules than epithelioid trophoblastic tumors

Gaspard Jeremie
Hospices Civils de Lyon
Fabienne Allias
Hospices Civils de Lyon
Alexis Trecourt
Hospices civils de Lyon
Lucie Gaillot-Durand
Hospices Civils de Lyon
Pierre-Adrian Bolze
Hospices Civils de Lyon
Françoise DESCOTES
Hospices Civils de Lyon
Garance TONDEUR
Hospices Civils de Lyon
Jimmy Perrot
groupment hospitalier lyon sud
Touria Hajri
Hospices Civils de Lyon
Benoit YOU
Institut de Cancérologie des Hospices Civils de Lyon https://orcid.org/0000-0002-3177-8857
François GOLFIER
Hospices Civils de Lyon
Jonathan Lopez
Hospices Civils de Lyon
Mojgan Devouassoux-Shisheboran (mojgan.devouassoux@chu-lyon.fr)
Hospices Civils de Lyon

Article

Keywords: Gestational trophoblastic disease, placental site nodule, atypical placental site nodule, epithelioid trophoblastic tumor, intermediate trophoblast, transcriptomic, gene signature.

Posted Date: August 26th, 2022

DOI: https://doi.org/10.21203/rs.3.rs-1978810/v1

Abstract

Gestational trophoblastic diseases derived from the chorionic-type intermediate trophoblast include benign placental site nodule (PSN) and malignant epithelioid trophoblastic tumor (ETT). Among PSN, the WHO classification introduced a new entity named atypical placental site nodule (APSN), corresponding to an ETT precursor, for which the diagnostic criteria remain unclear, leading to a risk of over-diagnosis and difficulties in patient management. We retrospectively studied 8 PSN, 7 APSN and 8 ETT to better characterize this new entity. We performed an immunohistochemical analysis (p63, hPL, Cyclin E, and Ki67), a transcriptional analysis using the Nanostring method to quantify the expression of 760 genes involved in the main tumorigenesis pathways, and a RNA sequencing to identify fusion transcripts.

The immunohistochemical analysis did not reveal any significant difference in Cyclin E expression between the three groups ($p = 0.476$), whereas the Ki67 index was significantly ($p < 0.001$) higher in ETT compared to APSN and PSN samples. None of the APSN samples harbored the *LPCAT1-TERT* fusion transcripts previously reported in ETT. The transcriptomic analysis allowed robust clustering of ETT distinct from the APSN/PSN group but failed to distinguish APSN from PSN. Indeed, only seven genes were differentially-expressed between PSN and APSN samples, *CCL19* upregulation and *EPCAM* downregulation were the most discriminating features of APSN. In contrast, 80 genes discriminated ETT from APSN, establishing a molecular signature for ETT. Gene set analysis identified significant enrichments in the DNA damage repair, immortality and stemness, and cell cycle signaling pathways when comparing ETT and APSN.

These results suggested that APSN might not represent a distinct entity but rather a variant of PSN or a transitional stage between PSN and ETT. RNA sequencing and the transcriptional signature of ETT described herein could serve as triage for APSN from curettage or biopsy material, enabling the identification of the cases that need further clinical investigations.

Introduction

Gestational trophoblastic disease (GTD) encompasses a heterogeneous group of lesions originating from intermediate trophoblasts and subdivided into several distinct entities, including true neoplastic proliferations such as choriocarcinoma, placental site trophoblastic tumor (PSTT), epithelioid trophoblastic tumor (ETT), and mixed trophoblastic tumor (MTT), as well as non-neoplastic tumor-like lesions such as exaggerated placental site reaction (EPSR) and placental site nodule (PSN)/atypical placental site nodule (APSN) (1). Over the last decades, the morphological and immunohistochemical analyzes of various GTD have shown that different intermediate trophoblastic lesions might derive from distinct subpopulations of intermediate trophoblast (IT) (2). PSTT and EPSR are thought to derive from the implantation site IT, while chorionic-type IT gives rise to ETT and PSN (3, 4).

PSN was initially described by Young *et al.* in 1990 (5). Subsequently, the morphological characteristics of this trophoblastic tumor-like lesion were detailed in several series, totalizing more than 100 cases (3, 5–7). None of the followed-up reported cases experienced adverse outcome after a simple curettage or hysterectomy, favoring a benign lesion (7). While PSN was thought to represent remnants of intermediate trophoblast from a previous gestation that has failed to completely involute, Shih and Kurman (2, 3) have described cases harboring intermediate features between typical PSN and ETT, characterized by a larger size (> 5 mm), an elevated Ki67 index (from 8–15%), and a higher cellularity compared to typical PSN, and have designated them as “atypical placental site nodule” (APSN). However, these lesions were benign in terms of prognosis. In 2015, Kaur *et al.* reported a series of 21 APSN cases from one of the three United Kingdom referral centers for GTD, 3 (14%) of which were associated with malignant GTD (ETT or PSTT), either concurrently or subsequently within 16 months of follow-up (8). APSN was introduced in the new WHO classification of female genital tract tumors in 2020 as an intermediate lesion between PSN and ETT and a putative precursor of ETT (1). However, definitive diagnostic criteria are not yet clearly established. While large size, increased cellularity, mitotic activity, and marked nuclear atypia should alert pathologists, the histological diagnosis of APSN from curettage specimen remains challenging (8–11). Although subjective, the diagnosis of APSN is based on morphological features, and very few ancillary techniques are available. The Ki67 proliferation index < 5% and the lack of Cyclin E immunoexpression are suggestive of PSN, while APSN harbors a 5–10% Ki67 index and Cyclin E positivity (12). Also, very few molecular analyses of IT lesions are available. A series investigating ETT using RNA sequencing has shown a high level of PD-L1 expression and an alteration of the PI3K pathway with frequent loss of PTEN expression (13). More recently, *LPCAT1-TERT* fusion transcripts and *TERT* amplification have been reported as characteristics of ETT that appear to be absent from PSN and PSTT (13, 14). However, APSN were not analyzed in these studies. Although prognosis, treatment, and clinical follow-up of APSN cases are still a matter of debate, some expert centers advocate for patients to undergo radiological workup and close follow-up or prophylactic hysterectomy (15). Thus, to avoid the over-diagnosis of APSN, there is a need for better diagnostic criteria.

This study aimed to investigate the active genes in chorionic-type IT lesions in order to correlate the transcriptomic signatures and histological type, define a possible progression from PSN to ETT via APSN, and finally provide molecular tools to help differentiate these lesions.

Materials And Methods

Patients’ selection:

All cases coded as trophoblastic tumors (except choriocarcinoma) or placental site nodule/plaque were retrospectively retrieved from the files of the department of pathology from the *Hospital, Hospices Civils de Lyon* between January 2012 and July 2021. During the study period, 30 PSTT, 12 ETT, 6 undifferentiated intermediate trophoblastic tumors, and 92 PSN (including 8 APSN) were obtained and were consultation cases in the vast majority (MDS, FA). Clinical and follow-up information were extracted from the French reference Center for Trophoblastic Disease database. The study was conducted according to the Declaration of Helsinki and approved by the local ethical committee and registered (N°21 5517).

Pathological selection of cases:

All Hematoxylin, Eosin, Saffron (HES) slides were reviewed independently by two senior pathologists (FA, MDS) to validate the diagnoses according to the WHO 2020 criteria (1). We defined APSN as PSN with a Ki67 index > 5% and ≥ 5 mm in size, and harboring at least one of the following WHO features: 1) cytological severe atypia, 2) increased cellularity with the presence of cohesive nests, 3) presence of any visible mitotic figure.

The study excluded one ETT reclassified as an undifferentiated intermediate trophoblastic tumor, one pulmonary ETT, and two ETT without available paraffin blocks. One case was a bladder recurrence 36 months after the initial uterine ETT, and we included the primary tumor and its recurrence in the study.

Among the 8 APSN cases, one was reclassified as PSN. This case was an incidentally-found 2-mm superficial nodule issued from the endometrial curettage of a 39-year-old infertile patient. The presence of nuclear atypia and mitotic figures and the 11% Ki67 were the criteria for our initial diagnosis as APSN. Upon review, the nodule was < 5 mm in size and the two “mitotic figures” were actually karyorrhectic nuclei (Fig. 1) such as those seen in uterine leiomyomas with bizarre nuclei (16). This case was included as a PSN with the 7 other PSN for which sufficient representative tissue material was left in the paraffin block, with at least 80% cellularity.

Ultimately, the molecular study was conducted on 8 PSN, 7 ETT (+ 1 bladder metastasis) and 7 APSN. We selected for each case a representative formalin-fixed paraffin-embedded (FFPE) tissue block for the immunohistochemical and molecular studies.

Immunohistochemistry:

The study was performed using Ventana Benchmark (Ventana-Roche, Meylan France) automated immunostainers with the following antibodies and according to the manufacturer's recommendations: Cyclin E (clone HE12, 1/500, Zymed, Invitrogen), p63 (clone 4A4, PAE, Ventana-Roche, Meylan France), hPL (human Placental Lactogen, clone PL, PAE, Cell Marque) and a double immunostaining AE1-AE3/Ki67 (clone 34βE12, 1/80, Dako and clone MIB1, 1/30, Dako, Les Ulis France). Nuclear staining with p63 and cytoplasmic staining with hPL were considered positive and evaluated using a semi-quantitative system. We calculated an H-score for Cyclin E by multiplying the intensity of staining (0–3) by the percentage of stained cells: H-score 1 for 0–10%, 2 for 11–50% and 3 for > 50%. The Ki67 proliferating index was calculated using Case Viewer software (2.0, 3DHISTOTECH Ltd, HUNGARY). Only AE1-AE3-labeled cells corresponding to trophoblastic cells were taken into account.

RNA extraction:

RNAs were extracted from FFPE samples following the macrodissection of tumor-cells-rich areas, and 2 to 6 5-µm slides were used depending on the size of the lesions. Slides were first dewaxed with two baths of D-Limonene (2 min) and a bath of Absolute Ethanol (2 min), and RNA extraction was then performed using HighPure FFPET RNA Isolation Kit (Roche, Switzerland, #06483852001).

Targeted transcriptomics and data analysis:

We conducted gene expression analysis using the NanoString nCounter FLEX platform (NanoString Technologies). We used the Tumor Signaling 360 panel (NanoString Technologies, USA, #XT-CSO-PROG1-12) targeting 760 genes related to 13 cancer-associated canonical pathways, including MAPK, STAT, PI3K, RAS, Cell Cycle, Apoptosis, Hedgehog, Wnt, DNA Damage Control, Transcriptional Regulation, Chromatin Modification, and TGF- . Depending on the concentrations, hybridization with Human Tumor Signaling 360 Panel probes was performed using 78 ng to 200 ng of RNA, according to the manufacturer’s instructions. After a 17–20h incubation at 65°C, samples were processed on a NanoString nCounter FLEX platform. Data were analyzed by ROSALIND® (https://rosalind.bio/) (San Diego, CA). Sample multidimensional scaling (MDS) plots were generated as part of the QC step. Normalization, fold changes, and p-values were calculated by dividing the counts within a lane by the geometric mean of the normalizer probes from the same lane. Housekeeping probes to be used for normalization were selected based on the geNorm algorithm as implemented in the NormqPCR R library. P-value adjustment was performed using the Benjamini-Hochberg method of estimating false discovery rates (FDR). We selected differentially expressed genes using a fold-change ≤ 2 and ≥ 2 and an FDR-adjusted p-value ≤ 0.05. The clustering of genes for the final heatmap of differentially expressed genes was performed using the PAM (Partitioning Around Medoids) method using the fpc R library. Hypergeometric distribution was used to analyze the enrichment of pathways, gene ontology, domain structure, and other ontologies.

RNAseq analysis:

We performed an RNAseq analysis to investigate presence of fusion transcripts, including the recently-described *LPCAT1::TERT* fusion. We used 21.2 to 214.8 ng of RNA to prepare libraries according to the Archer Fusion-Plex Protocol for Illumina (ArcherDX Inc., San Diego, CA) instructions. We used an in-house pan-cancer sequencing panel (RNA Seq ARCHER Panel FusionPlex_CHU_Lyon_Pan_Solid_Tumor _Sarcoma_17125-v1.0). Data analysis was performed using the Archer Analysis software (v6.2; ArcherDX Inc.). One additional ETT sample harboring the *LPCAT1:TERT* fusion was used as a positive control.

Results

A total of 8 PSN, 7 ETT (+ 1 bladder metastasis) and 7 APSN samples were included in the study.

Clinical presentation:

In the PSN group, the mean (range) age of patients was 36.1 (29–43) years. The interval from the most recent known pregnancy to the time of presentation was known for three patients and ranged from two weeks to 72 months. Serum hCG level was known for two patients and was within normal range. All PSN were intrauterine and superficially located on the surface of the endometrium, with focal superficial myometrial extension in one case. Patients presented vaginal bleeding in 6 cases, infertility in one case, and one patient was asymptomatic. None of the PSN patients was followed-up, except the case with karyorrhectic nuclei on endometrial curettage, and this patient was well 91 months after the diagnosis.

The mean (range) age of patients from the APSN group was 34.8 (25–46) years (Table 1).

Table 1
Clinical and histopathological characteristics of the 7 atypical placental site nodules (APSN).

APSN	Age Years	Symptoms	hCG IU/ml	Time since last pregnancy (months)	Procedure	Size mm	Location	High cellularity	Mitoses /mm2	Severe Atypia	Tumor cell Necrosis	Ki67 %	F u (r
1	29	Menorrhagia	NA	6	Curettage	7	Cervix	Yes	0.29	No	No	15	N re (7
2	25	Amenorrhea	NA	18	Curettage	11	Endometrium	Yes	0	No	Yes	16	L fo u
3	32	Pelvic pain	NA	NA	Hysterectomy	11	Isthmus	No	0.29	No	No	8	L fo u
4	30	Pelvic pain	0	NA	Salpingectomy	40	Tubal cyst	Yes	0	Yes	Yes	10	L fo u
5	46	Menorrhagia	0	20	Curettage	6	Endometrium	Yes	0.29	No	Yes	12	N re (2
6	36	Menorrhagia	NA	20	Curettage	9	Isthmus	No	0.29	No	Yes	8	N re (2
7	46	Menorrhagia	0	30	Hysterectomy	14	Endometrium	Yes	0	Yes	Yes	13	N re (1

Abbreviations : APSN, atypical placental site nodule; NA : not available ; hCG, human chorionic gonadotropin

In the ETT group, the patient mean (range) age was 47.7 (33–62) years. The mean (range) interval between the preceding gestational event (none of which was molar pregnancy) and the diagnosis was 187.5 (60–304) months. All patients presented bleeding, in addition to pelvic pain for three patients. A total of 5 (71%) patients had normal hCG levels, and two had elevated levels (118 and 1284 IU/ml). All patients were treated by total hysterectomy, and three also received adjuvant chemotherapy. The metastatic ETT was secondarily treated by cystectomy. Tumors were limited to the uterine corpus (4/7) or showed cervical invasion (1/7), ovarian metastasis (1/7), or peritoneal extension with lung metastasis (1/7) that were resected during initial surgery. After a mean (range) follow-up duration of 40 (3-111) months, all patients were alive and disease-free, except for one patient experiencing a bladder recurrence 36 months after the initial diagnosis that was resected and included in the molecular analysis.

Histological features:

In the PSN group (Fig. 1A, 1B), the mean (range) size of the nodule was 3.8 (2–8) mm. All PSNs were composed of isolated cells or very small trabeculae with eosinophilic cytoplasm with nuclear hyperchromasia and bizarre nuclear shapes and multinucleated cells in a background of hyaline tissue. In one case, two karyorrhectic nuclei were observed (Fig. 1C, 1D).

The mean size of the nodule was 14 mm in the APSN group (Table 1). The largest was a 40-mm paratubal cyst with a highly cellular rim 3-mm thick (Figs. 1E, 1F). The cellularity was higher than for PSN, with cells arranged in cohesive nests in a background of hyaline tissue. Fibrinoid and amorphous hyaline necrosis were observed in all cases, but typical tumor cell necrosis was detected in only 5 cases (Fig. 1E, 1F). All cases exhibited nuclear atypia with large and irregular nuclei, but two cases displayed extensive severe nuclear atypia.

In the ETT group (Fig. 1G, 1H), the mean (range) tumor size was 25 (6–80) mm. Tumor cells were arranged in cords and solid nests, with moderate nuclear atypia. Severe nuclear atypia was focally seen in three cases. Tumor cell necrosis was identified in 6 cases displaying an irregular and geographic pattern. The mean (range) mitotic count was 1.7 (0.58–4.11) mitoses/mm^2. One case of ETT was associated with an APSN adjacent to the tumor. The initial ETT and bladder recurrence displayed the same morphological aspect with 2.3 and 2.7 mitoses/mm^2, respectively.

Immunohistochemical study:

P63 nuclear staining was moderate to strong in all cases (PSN, APSN, and ETT), while hPL was negative or very focally positive in 4/8 PSN, 6/7 APSN, and 4/7 ETT samples. The mean (range) Ki67 index was 4.8 (1–11) %, 11.7 (8–16) %, and 20 (14–26) % in the PSN, APSN, and ETT groups, respectively, and differed significantly between groups ($p < 0.001$; Fig. 2A). The mean (range) cyclin E H-score was 91 (20–150), 122 (10–180), and 129 (20–230) in the PSN, APSN, and ETT groups, respectively, and did not differ significantly between groups ($p = 0.476$; Fig. 2B).

Transcriptomic analysis of PSN, APSN, and ETT samples:

First, we performed multidimensional scaling (MDS) on the normalized NanoString counts for the graphical representation of relationships between the three groups. ETT samples clustered together on one side, APSN and PSN samples clustered on the other side, and the two latter sample types partially overlapped.

Interestingly, most of the APSN samples had an intermediate position between PSN and ETT (Fig. 3).

Differential-expression analysis identify only 7 genes when comparing APSN to PSN samples (Supplementary Table 1 and Fig. 4). However, these seven genes failed to discriminate APSN from PSN samples in hierarchical clustering, confirming the MDS plot. The 2 most discriminating genes were *CCL19* and *EPCAM*. *CCL19* expression was increased 20 times in APSN samples compared to PSN samples (p-Adj = 0.034), whereas *EPCAM* was decreased by 6 times in APSN samples compared to PSN samples (p-Adj = 0.044; Fig. 4).

Then we compared ETT and APSN samples and identified 80 differentially-expressed genes (Supplementary Table 2 and Fig. 5). This gene-expression signature efficiently discriminated ETT from APSN samples. The 2 most discriminating genes were *CCNE1* and *KIR2DL3*. *CCNE1* expression was increased 5 times in ETT samples compared to APSN samples (p-Adj = 0.035) whereas *KIR2DL3* was decreased by 15 times in ETT samples compared to APSN samples (p-Adj = 0.006; Fig. 5).

Gene set analysis identified significant enrichments in ETT samples compared to APSN samples in DNA damage repair (17 genes), immortality and stemness (10 genes), and cell cycle (33 genes) pathways ($p < 0.001$).

RNA sequencing

We found no *LPCAT1:TERT* fusion among the 7 APSN samples, 2 PSN samples (including the sample from a case with karyorrhectic nuclei), and one ETT sample.

Discussion

Genomic characteristics are little known in the context of GTD, particularly for ETT and its putative precursor, APSN. Here, we found that gene expression analysis efficiently discriminated ETT from placental site nodules (APSN + PSN) but failed to distinguish APSN from PSN.

Based on our results, APSN may not represent a distinct entity but rather a variant of PSN or a transitional stage between PSN and ETT. This may explain why it seems so difficult to find reproducible and objective histological criteria enabling the classification of PSN and its distinction from APSN, while the histological diagnosis and distinction between PSN and ETT is more straightforward. The continuum between PSN, APSN, and ETT has already been described in published studies using a morphological perspective. Indeed, in 2008, one case report has described the transformation of a PSN into an APSN and then into an ETT (11) showing an increase in cellularity, gradual severity of the cytonuclear atypia, and an increase in the mitotic index between PSN and ETT with a transition zone, within which the Ki67 index increased gradually corresponding to an APSN zone. Two other case reports have described the close association between a typical PSN and an APSN and their transformation into an ETT, but also into a PSTT (9, 19).

The NanoString analysis identified 80 differentially-expressed genes between ETT and APSN, while we observed seven differentially-expressed genes only, between PSN and APSN. Interestingly, *CCL19* expression was increased 20 times and *EPCAM* expression was downregulated 6 times in APSN compared to PSN. Increased expression of *CCL19* has been associated with progression in the context of cervical cancer and both increased *CCL19* expression and *EPCAM* downregulation have been related to the epithelial-mesenchymal transition (EMT) phenomenon (20). However, our research group has failed to detect EMT features in gestational trophoblastic neoplasms (21).

ETT is the rarest form of GTD, composed of chorionic-type IT, which has a potential for metastasis (25% of cases). Although PSN is also composed of chorionic-type IT, it is benign. APSN has been described as an intermediate lesion between PSN and ETT that can be associated with or progress to a true neoplasm (ETT or PSTT) in 14% of cases (8). It is considered as an uncommon lesion representing 0.5% of GTD cases in the study by Kaur *et al.* (8) and herein 0.2% of GTD (7/3504) cases and 8% of PSN (7/92) during the study period in our department (one of the 8 pathology department reviewing cases for the French Referral Center for Trophoblastic Disease). Except for one report including 21 cases, APSN has been described as case reports only (9–11, 17). The present study is the second series including 7 APSN, and no adverse outcome was reported for 4 cases that were followed-up for 7 to 34 months.

PSN and APSN may present overlapping pathological features, and the morphological characteristics criteria of APSN are not well established. Large size, atypical cells, and mitoses are criteria for distinguishing APSN from PSN. However, large and plaque-like nodules and multinucleated and bizarre nuclei have been initially described in all PSN series, and no adverse outcome has been reported (5–7). Necrosis is a characteristic feature of PSN, usually described as eosinophilic amorphous or fibrinoid necrosis with hyalinization in the center of nodules in a PSN. Tumor cell necrosis is difficult to assess from the morphology alone and is related to considerable interobserver variability, as described for uterine smooth muscle (18); and we did not use necrosis as a criterion for distinguishing PSN from APSN. Although mitotic figures are usually inexistent in PSN, up to 3 mitoses per 10 high power fields have been reported. These cases, including 5 of 7 cases with mitoses in the series by Huettner *et al.* (7), progressed well over the follow-up. One of our findings was the presence of possible karyorrhectic cells characterized by dense eosinophilic cytoplasm surrounded by retraction and coarse fragmented chromatin that may mimic atypical mitosis in PSN. Degenerative cytologic changes are common in PSN, reminiscent of what is observed in uterine leiomyomas with bizarre nuclei in which karyorrhectic modifications are well known and are not interpreted as mitotic figures (16). Confirming that karyorrhexis is not a criterion for diagnosing APSN, this particular case displayed a molecular signature closer to PSN than ETT. Ki67 index has been used as a tool for distinguishing PSN (< 5%) from APSN (5–10%). Herein, we confirmed the utility of Ki-67 index that could significantly distinguish PSN from APSN and ETT. We should emphasize that karyorrhectic figures were stained with Ki67. Contrary to a previous study (12), we showed that Cyclin E immunoexpression was not reliable enough to distinguish these three entities. Also, the *CCNE1* (Cyclin E1) gene was not differentially expressed between the three groups, despite being overexpressed in ETT compared to APSN at the mRNA level.

Recently, *LPCAT1:TERT* fusion has been demonstrated to be specific of ETT, and absent from PSN and PSTT (14). Herein, none of the seven APSN samples harbored a *LPCAT1:TERT* fusion transcript. This could represent a marker favoring the diagnosis of ETT rather than APSN from curetting material. Indeed, a

proportion of APSN might represent true ETT insufficiently sampled by curettage. The identification of *LPCAT1:TERT* fusion transcript and the transcriptional signature of ETT by NanoString described herein should incite the investigation of a tumor mass with MRI, favoring ETT rather than APSN.

In conclusion, these results suggested that APSN might not represent a distinct entity but rather a variant of PSN challenging to characterize based on morphology and ancillary techniques, and supported the idea of a continuum spectrum of IT lesions, from PSN to APSN and then to ETT. While a diagnosis of PSN does not implicate follow-up, the clinical management of APSN is not yet codified, and it is unclear whether hysterectomy or repeated imaging is necessary. The transcriptional signature described herein, as well as the presence of the *LPCAT1:TERT* fusion transcript, could serve as triage among APSN cases, identifying the cases that require further clinical investigations. However, the transcriptional signature of ETT reported herein needs to be validated with an independent multicenter cohort study.

Declarations

Author contributions

Data analysis, writing of the original manuscript: G Jeremie, M Devouassoux-Shisheboran, F Allias, J Lopez, L Gaillot-Durand

NanoString and molecular analysis: J Lopez, F Descotes, G Tondeur, J Perrot

Contribution to the clinical follow-up : PA Bolze, F Golfier, B You

Database contribution: T Hajri

Critical analysis: A Trecourt

Declaration of interest

The authors declare no conflict of interest

Acknowledgements and funding

This study was financially supported by the Cellule Recherche of the Biology and Pathology Medical Pole, Hospices Civils de Lyon.

The authors would like to thank Hélène Boyer (Hospices Civils de Lyon) for help in manuscript preparation and English editing.

References

1. Who-Classification-Of-Tumours/Female-Genital-Tumours., Lyon France IARC -2020
2. Shih IM, Kurman RJ. The pathology of intermediate trophoblastic tumors and tumor-like lesions. Int J Gynecol Pathol 20,31-47(2001).
3. Shih I ming, Seidman JD, Kurman RJ. Placental site nodule and characterization of distinctive types of intermediate trophoblast. Hum Pathol. 30,687-94 (1999).
4. Shih IM, Kurman RJ. Molecular basis of gestational trophoblastic diseases. Curr Mol Med. 2,1-12 (2002).
5. Young RH, Kurman RJ, Scully RE. Placental site nodules and plaques. A clinicopathologic analysis of 20 cases. Am J Surg Pathol. 14,1001-9 (1990).
6. Santos LD, Fernando SSE, Yong JLC, Killingsworth MC, Juan Wu X, Kennerson AR. Placental site nodules and plaques: a clinicopathological and immunohistochemical study of 25 cases with ultrastructural findings. Pathology 31,328-36 (1999).
7. Huettner PC, Gersell DJ. Placental site nodule: a clinicopathologic study of 38 cases. Int J Gynecol Pathol Off J Int Soc Gynecol Pathol.13,191-8 (1994).
8. Kaur B, Short D, Fisher RA, Savage PM, Seckl MJ, Sebire NJ. Atypical placental site nodule (APSN) and association with malignant gestational trophoblastic disease, a clinicopathologic study of 21 cases. Int J Gynecol Pathol 34,152-8 (2015).
9. Dholakia J, Chen W, O'Malley DM, Ronnett BM. A Rare Case of Atypical Placental Site Nodule With an Emerging Intermediate Trophoblastic Tumor. Int J Gynecol Pathol 39, 238-46 (2020).
10. McCarthy WA, Paquette C, Colavita M, Lawrence WD. Atypical Placental Site Nodule Arising in a Postcesarean Section Scar: Case Report and Review of the Literature. Int J Gynecol Pathol 38, 71-5 (2019).
11. Tsai HW, Lin CP, Chou CY, Li CF, Chow NH, Shih IM, et al. Placental site nodule transformed into a malignant epithelioid trophoblastic tumour with pelvic lymph node and lung metastasis. Histopathology. 53, 601-4 (2008).
12. Mao TL, Seidman JD, Kurman RJ, Shih IM. Cyclin E and p16 immunoreactivity in epithelioid trophoblastic tumor–an aid in differential diagnosis. Am J Surg Pathol. 30, 1105-10 (2006).
13. Cho EJ, Chun SM, Park H, Sung CO, Kim KR. Whole transcriptome analysis of gestational trophoblastic neoplasms reveals altered PI3K signaling pathway in epithelioid trophoblastic tumor. Gynecol Oncol. 157, 151-60 (2020).
14. Oliver GR, Marcano-Bonilla S, Quist J, Tolosa EJ, Iguchi E, Swanson AA, et al. LPCAT1-TERT fusions are uniquely recurrent in epithelioid trophoblastic tumors and positively regulate cell growth. PLoS ONE. 16, e0250518 (2021).
15. Clark JJ, Slater S, Seckl MJ. Treatment of gestational trophoblastic disease in the 2020s. Curr Opin Obstet Gynecol. 33, 7-12 (2021).
16. Croce S, Young RH, Oliva E. Uterine leiomyomas with bizarre nuclei: a clinicopathologic study of 59 cases. Am J Surg Pathol. 38, 1330-9 (2014).
17. Yen TT, Anderson J, Shih IM. Case Report: Tubal Atypical Placental Site Nodule. Int J Gynecol Pathol 41,230-534 (2022).

18. Lim D, Alvarez T, Nucci MR, Gilks B, Longacre T, Soslow RA, et al. Interobserver variability in the interpretation of tumor cell necrosis in uterine leiomyosarcoma. Am J Surg Pathol. 37, 650-8 (2013).
19. Chen BJ, Cheng CJ, Chen WY. Transformation of a post-cesarean section placental site nodule into a coexisting epithelioid trophoblastic tumor and placental site trophoblastic tumor: a case report. Diagn Pathol. 8, 85 (2013).
20. Zhang X, Wang Y, Cao Y, Zhang X, Zhao H. Increased CCL19 expression is associated with progression in cervical cancer. Oncotarget. 8, 73817-73825 (2017).
21. Dubruc E, Allias F, Morel AP, Golfier F, Puisieux A, Devouassoux-Shisheboran M. Gestational trophoblastic neoplasms (GTNs) do not display epithelial-to-mesenchymal transition (EMT) features. Virchows Arch. 475, 121-125 (2019).

Figures

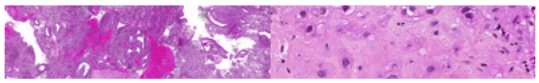

Figure 1

Representative histologic images of Hematoxylin, Eosin, Saffron staining.

A, B: Placental site nodule. Well-circumscribed small nodular lesion located at the surface of the endometrial mucosa and composed of chorionic-type intermediate trophoblastic cells dispersed as isolated cells with clear or eosinophilic cytoplasm and round nuclei embedded in a hyalinized matrix.

C, D: Placental site nodule. Well-circumscribed small lesion superficially located at the surface of the endometrium showing large, irregular, and hyperchromatic dystrophic-looking nuclei with karyorrhectic image (Arrow).

E, F: Atypical placental site nodule. Large cystic lesion centered by hemorrhage and necrosis with a cellular rim showing hypercellularity and nests of chorionic-type intermediate trophoblastic cells with atypia and necrosis.

G, H: Epithelioid trophoblastic tumor. Large nests of tumor cells with abundant geographic necrosis and preservation of viable tumor cells in a perivascular arrangement, with round and polygonal cells displaying relatively uniform round nuclei, small nucleoli, and mitotic figures.

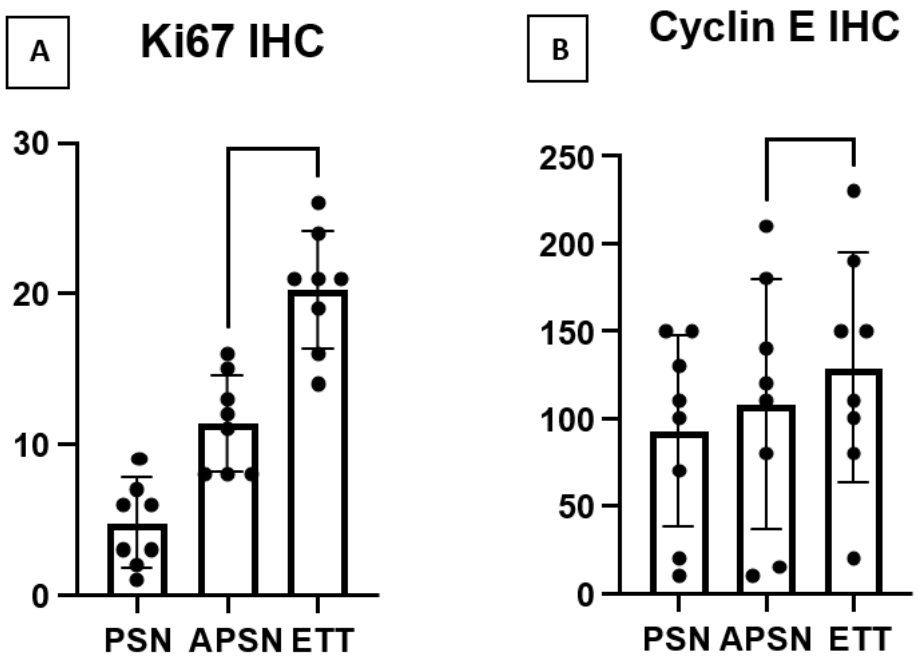

Figure 2

Ki67 index and Cyclin E expression studied by immunohistochemistry in PSN (Placental Site Nodule), APSN (Atypical Placental Site Nodule), and ETT (Epithelioid Trophoblastic Tumor) samples. 2A: Ki67 index was significantly different between these 3 groups ($p < 0.001$). The mean (range) Ki67 index was 4.8 (1-11) %, 11.7 (8-16) %, and 20 (14-26) % in the PSN, APSN, and ETT groups, respectively. 2B: Cyclin E expression, evaluated using the H-Scoring system, was not statistically different between these 3 groups ($p = 0.476$). The mean (range) cyclin E H-score was 91 (20-150), 122 (10-180), and 129 (20-230) in the PSN, APSN, and ETT groups, respectively.

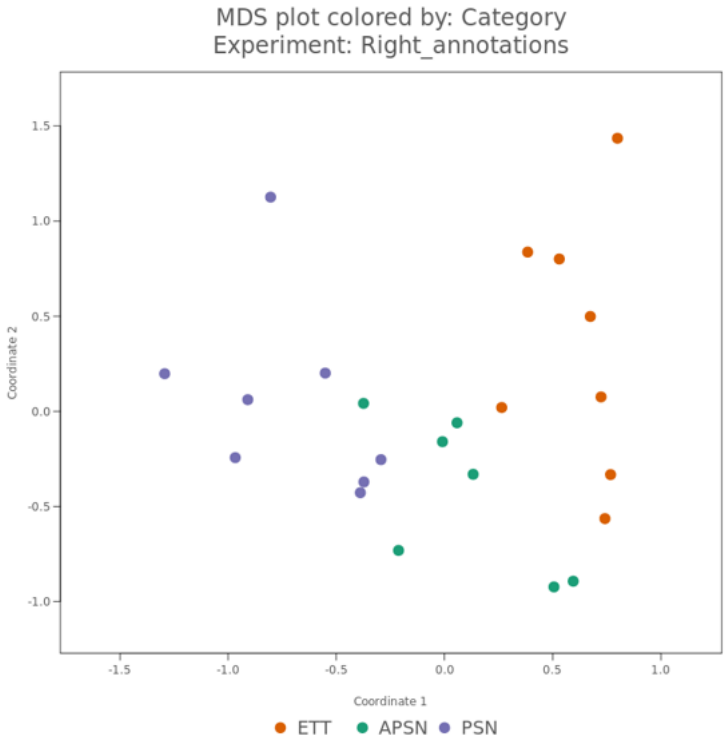

Figure 3

Multidimensional scaling (MDS) plot of individual cases of the transcriptomic data. ETT (Epithelioid Trophoblastic Tumor) samples are represented in red, APSN (Atypical Placental Site Nodule) in green, and PSN (Placental Site Nodule) in blue.

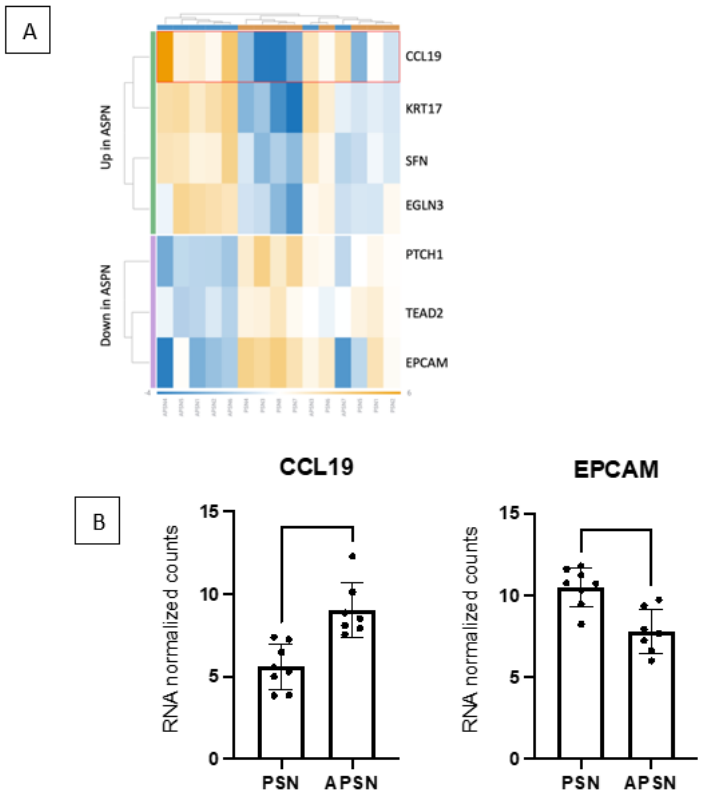

Figure 4

Differentially-expressed genes (DEG) between PSN (Placental Site Nodule) and APSN (Atypical Placental Site Nodule) samples. 4A: hierarchical clustering based on the 7 DEG (fold change>2, p-Adj<0.05). PSN samples are represented in orange and APSN samples in blue. 4B: bar graphs representing *CCL19* and *EPCAM* expression in PSN and APSN samples. *** p<0.001, ** p<0.01.

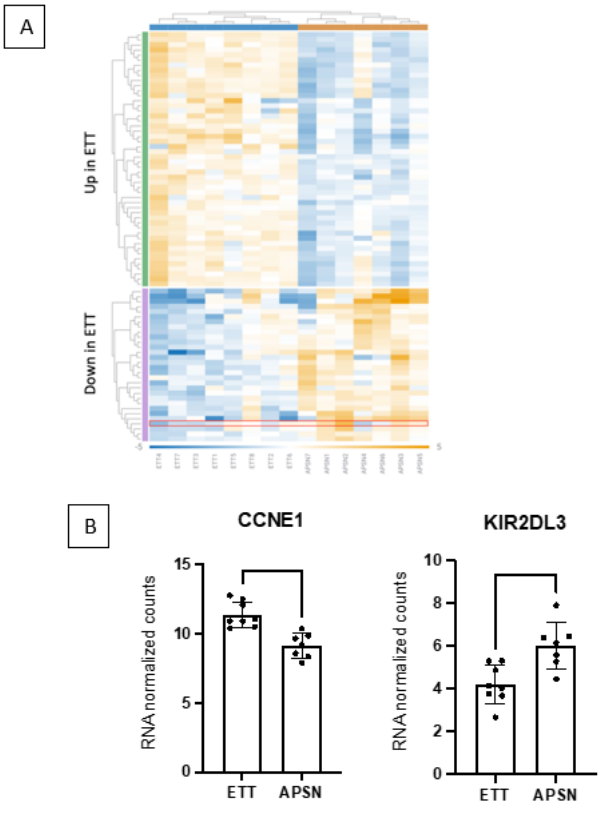

Figure 5

Differentially-expressed genes (DEG) between APSN (Atypical Placental Site Nodule) and ETT (Epithelioid Trophoblastic Tumor) samples. 5A: hierarchical clustering based on the 80 DEG (fold change>2, p-Adj<0.05). APSN samples are represented in orange and ETT samples in blue. 5B: bar graphs representing *CCNE1* and *KIR2DL3* expression in ETT and APSN samples. *** p<0.001, ** p<0.01.

Supplementary Files

This is a list of supplementary files associated with this preprint. Click to download.

- SupplementaryTable1APSNvsPSN.xlsx
- SupplementaryTable2ETTvsAPSN.xlsx